NeuroImage 51 (2010) 531–541

Contents lists available at ScienceDirect

NeuroImage

journal homepage: www.elsevier.com/locate/ynimg

Microstructural correlations of white matter tracts in the human brain

Michael Wahl [a,b], Yi-Ou Li [a], Joshua Ng [a], Sara C. LaHue [a], Shelly R. Cooper [a], Elliott H. Sherr [b], Pratik Mukherjee [a,c,*]

[a] Department of Radiology and Biomedical Imaging, University of California, San Francisco, CA, USA
[b] Department of Neurology, University of California, San Francisco, CA, USA
[c] Department of Bioengineering and Therapeutic Sciences, University of California, San Francisco, CA, USA

ARTICLE INFO

Article history:
Received 31 October 2009
Revised 10 February 2010
Accepted 25 February 2010
Available online 4 March 2010

Keywords:
Behavior
Brain
Cognition
Diffusion tensor imaging (DTI)
Human
Hierarchical clustering
Fiber tractography
Language
White matter

ABSTRACT

The purpose of this study is to investigate whether specific patterns of correlation exist in diffusion tensor imaging (DTI) parameters across different white matter tracts in the normal human brain, and whether the relative strengths of these putative microstructural correlations might reflect phylogenetic and functional similarities between tracts. We performed quantitative DTI fiber tracking on 44 healthy adult volunteers to obtain tract-based measures of mean diffusivity (MD), fractional anisotropy (FA), axial diffusivity (AD), and radial diffusivity (RD) from four homologous pairs of neocortical association pathways (arcuate fasciculi, inferior fronto-occipital fasciculi, inferior longitudinal fasciculi, and uncinate fasciculi bilaterally), a homologous pair of limbic association pathways (left and right dorsal cingulum bundles), and a homologous pair of cortical–subcortical projection pathways (left and right corticospinal tracts). From the resulting inter-tract correlation matrices, we show that there are statistically significant correlations of DTI parameters between tracts, and that there are statistically significant variations among these inter-tract correlations. Furthermore, we observe that many, but by no means all, of the strongest correlations are between homologous tracts in the left and right hemispheres. Even among homologous pairs of tracts, there are wide variations in the degree of coupling. Finally, we generate a data-driven hierarchical clustering of the fiber pathways based on pairwise FA correlations to demonstrate that the neocortical association pathways tend to group separately from the limbic pathways at trend-level statistical significance, and that the projection pathways of the left and right corticospinal tracts comprise the most distant outgroup with high confidence ($p<0.01$). Hence, specific patterns of microstructural correlation exist between tracts and may reflect phylogenetic and functional similarities between tracts. The study of these microstructural relationships between white matter pathways might aid research on the genetic basis and on the behavioral effects of axonal connectivity, as well as provide a revealing new perspective with which to investigate neurological and psychiatric disorders.

Introduction

Since its introduction over 15 years ago, diffusion tensor imaging (DTI) has enabled the noninvasive assessment of the microstructural organization of human white matter pathways in health and disease (Basser and Pierpaoli, 1996; Pierpaoli et al., 1996). With the more recent advent of quantitative DTI fiber tractography (Conturo et al., 1999; Mori et al., 1999; Basser et al., 2000), it is now possible to reproducibly measure DTI parameters such as mean diffusivity, (MD), fractional anisotropy (FA), axial diffusivity (AD), and radial diffusivity (RD) over the three-dimensional course of many white matter tracts (Wakana et al., 2007). Measurements of DTI parameters from regions of interest within white matter as well as from entire tracts have been shown to correlate with cognitive and other behavioral performance, often with specific microstructure–function relationships in particular white matter tracts (Klingberg et al., 2000; Beaulieu et al., 2005; Tuch et al., 2005; Niogi and McCandliss 2006; Niogi et al., 2008b; Zahr et al., 2009). Decreases in the microstructural integrity of white matter pathways have been found for many neurologic and psychiatric disorders, often correlating with clinical and neurocognitive deficits in these patients (Klingberg et al., 2000; Niogi and McCandliss 2006; Niogi et al., 2008b).

While there has been rapid growth in the understanding of how the microstructural organization of specific white matter pathways correlates with behavior, to our knowledge there has not been a systematic examination of whether quantitative DTI parameters of different tracts co-vary with each other across individuals. The assumption implicit in many DTI studies is that a particular metric such as FA is independent across white matter tracts; hence, each

* Corresponding author. Neuroradiology Section, Department of Radiology and Biomedical Imaging, University of California, San Francisco, 505 Parnassus Avenue, Box 0628, San Francisco, CA 94143-0628, USA. Tel.: +1 415 353 1639; fax: +1 415 353 8593.
E-mail address: pratik@radiology.ucsf.edu (P. Mukherjee).

1053-8119/$ – see front matter © 2010 Elsevier Inc. All rights reserved.
doi:10.1016/j.neuroimage.2010.02.072

pathway is analyzed separately with respect to its contribution to cognitive ability. Conversely, different tracts may be treated as if they were equivalent, such as when measurements in homologous tracts of the left and right hemispheres are averaged or when the contralateral tract is used as a control for the homologous tract ipsilateral to the pathology in clinical studies of disorders presumed to be unilateral. But the precise degree to which microstructural covariances exist between tracts is largely unknown. Several prior studies have reported hemispheric asymmetries in homologous pairs of fiber pathways using DTI in healthy adults (Gong et al., 2005; Powell et al., 2006; Rodrigo et al., 2007), in the developing human brain (Bonekamp et al., 2007; Wilde et al., 2009), and in the aging human brain (Li et al., 2009; Yasmin et al., 2009), but these studies have focused on group differences in the mean value of DTI parameters rather than on assessing their correlation.

The purpose of this study is to investigate whether specific patterns of correlation exist in DTI parameters across white matter tracts in the normal adult human brain, and whether the strength of these putative correlations might reflect phylogenetic and functional similarities between tracts. To this end, we examined tract-based measures of MD, FA, AD, and RD from four pairs of neocortical association pathways (arcuate fasciculi, inferior fronto-occipital fasciculi, inferior longitudinal fasciculi, and uncinate fasciculi bilaterally), a pair of limbic association pathways (bilateral dorsal cingulum bundles), and a pair of cortical–subcortical projection pathways (bilateral corticospinal tracts), following the tract terminology of Mori et al. (2005). From the resulting inter-tract correlation matrices, we investigate whether there are statistically significant correlations of DTI parameters between tracts, and whether there are statistically significant variations among these inter-tract correlations. We specifically examine if correlations between homologous pairs of tracts always exceed those between non-homologous tracts. Finally, we perform a data-driven hierarchical clustering analysis of pairwise DTI correlations to group tracts based on their microstructural relatedness, using the results to test the hypothesis that microstructural correlations reflect phylogenetic and functional similarities between white matter pathways.

Materials and methods

Participants

The inclusion criteria for subjects in this study were healthy volunteers ages 20–50 years. Exclusion criteria included any history of chronic medical illness, neurological or psychiatric disorder, including substance abuse, as well as any contraindications to MR imaging including pregnancy. Any brain morphological abnormalities found on structural MR imaging also constituted an exclusion criterion. Written informed consent was obtained from all participants in accordance with protocols approved by the institutional review board of the University of California, San Francisco. There were a total of 44 subjects (mean age 30.8 ± 7.8 years, 24 men and 20 women, 35 right-handed and 9 left-handed) enrolled who met all inclusion and exclusion criteria.

MRI and DTI acquisition

Magnetic resonance imaging was acquired on a 3 T Signa EXCITE scanner (GE Healthcare, Waukesha, WI) equipped with an 8-channel phased-array head coil. Whole-brain DTI was performed with a multi-slice single-shot spin echo echoplanar pulse sequence (TE = 63 ms, TR = 14 s) using 55 diffusion-encoding directions, isotropically distributed over the surface of a sphere with electrostatic repulsion, acquired at $b = 1000\ \mathrm{s/mm^2}$, 1 acquisition with $b = 0\ \mathrm{s/mm^2}$, 72 interleaved axial slices oriented along the anterior commissure–posterior commissure (AC-PC) line, 1.8-mm slice thickness with no gap between slices, a 128 × 128 matrix and a field of view (FOV) of 230 mm. To reduce echoplanar image distortion, parallel imaging was employed using the Array Spatial Sensitivity Encoding Technique (ASSET) with an acceleration factor of 2. Total acquisition time was 13.07 min. The signal-to-noise ratio (SNR) was in the range of 18–33 on the $b = 0\ \mathrm{s/mm^2}$ images, as calculated using the difference method that has been shown by Dietrich et al. (2007) to be the most accurate for parallel imaging acquisitions. Higher SNR was found in superficial regions and lower SNR in deeper regions of the brain, reflecting variations in sensitivity of the multichannel phased array head coil.

High-resolution structural 3 T MR imaging was performed using an axial 3D inversion recovery fast spoiled gradient-recalled echo (FSPGR) T1-weighted sequence (TE = 1.5 ms, TR = 6.3 ms, TI = 400 ms, flip angle of 15°) with 230 mm FOV, 156 1.0-mm contiguous partitions at a 256 × 256 matrix.

DTI processing and tractography

After non-brain tissue was removed using the Brain Extraction Tool (BET; http://www.fmrib.ox.ac.uk/analysis/research/bet/) with a fractional intensity threshold of 0.3 (Smith, 2002), the diffusion-weighted images were corrected for motion and eddy currents using FMRIB's Linear Image Registration Tool (FLIRT; www.fmrib.ox.ac.uk/fsl/flirt) with 12-parameter linear image registration (Jenkinson et al., 2002). All diffusion-weighted images were registered to the unweighted $b = 0\ \mathrm{s/mm^2}$ image. Images were post-processed offline in DTIstudio v2.4 software (Jiang et al., 2006) using multivariate linear fitting to obtain maps of FA, MD, AD, RD, and directionally-encoded color FA. Tractography was performed with Fiber Assignment by Continuous Tracking (Mori et al., 1999), using the brute-force method in which tracks were seeded from all voxels in the brain with an FA value larger than 0.3. Fibers were tracked while voxel FA values exceeded 0.2 and turning angles of the primary eigenvectors between neighboring voxels were less than 50°. These fiber tracking parameters are similar to other recent quantitative DTI tractography studies of the normal adult brain (Reich et al., 2006; Rodrigo et al., 2007; Wakana et al., 2007; Danielian et al., 2010). Individual tracts were then selected by requiring fibers to pass through manually placed Regions of Interest (ROIs) on DTI color maps, according to protocols specific for each tract, as described by Wakana et al. (2007) and implemented in DTIstudio. Any anatomically implausible fibers were removed using exclusion ROIs, as also described by Wakana et al. (2007). Quantitative tract-based measurements of FA, MD, AD, and RD were obtained for six axonal pathways bilaterally, specifically the arcuate fasciculus (AF), dorsal cingulate bundle (CB), corticospinal tract (CST), inferior fronto-occipital fasciculus (IFO), inferior longitudinal fasciculus (ILF) and uncinate fasciculus (UF). Mid-sagittal projections of the three-dimensional course of the left-sided tracts are illustrated in Fig. 1. Our terminology differs from that of Wakana et al. (2007) in that they refer to the arcuate fasciculus as the "temporal component of the superior longitudinal fasciculus" and they refer to the dorsal cingulum as the "cingulum in the cingulate gyrus part". Since spatial overlap of tracts would influence their microstructural correlation, the degree of overlap was quantified for each tract pair within the same hemisphere in 25 consecutive subjects as the percentage of shared voxels. This is calculated as follows: let V_A be the number of voxels contained within tract A, V_B be the number of voxels within tract B, and V_{AB} be the total number of voxels within tracts A and B where voxels contained within both tracts are counted only once. Then $100\% \times (V_A + V_B - V_{AB}) / (V_A + V_B)$ represents the percentage of shared voxels between tracts A and B.

DTI correlation analysis

The distributions of FA values of each set of p = 12 tracts across the 44 subjects did not differ from normality using the Shapiro–Wilk test, except for FA of the left UF which showed a statistically significant deviation from normality ($p < 0.05$). However, MD values in 8 of the 12

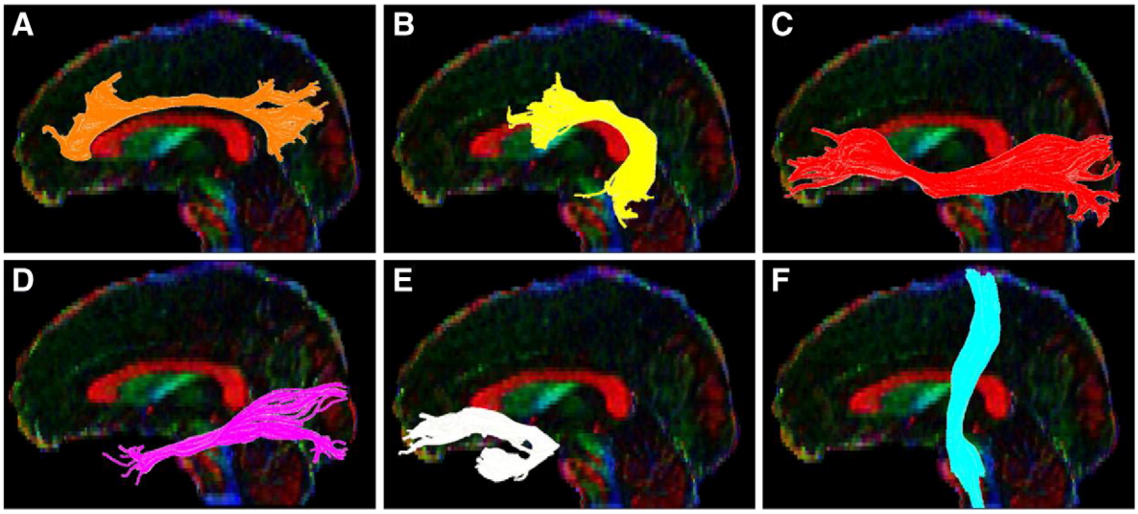

Fig. 1. Mid-sagittal projections of 3D DTI fiber tracking of the (A) dorsal cingulate bundle; (B) arcuate fasciculus; (C) inferior fronto-occipital fasciculus; (D) inferior longitudinal fasciculus; (E) uncinate fasciculus; and (F) corticospinal tract. The fiber tracts are overlaid on directionally-encoded color fractional anisotropy images of a healthy volunteer.

tracts showed significant departures from normality ($p<0.05$). There were no deviations from normality for AD values in any of the 12 tracts ($p>0.05$), but the distribution of RD values differed significantly from Gaussian in 6 of the 12 tracts ($p<0.05$). Hence, the nonparametric Spearman's rank correlation coefficient ρ was used to measure all correlations. A correlation matrix was constructed for each of the 4 DTI parameters using pairwise correlation values between tracts. The correlation matrices are symmetric and have values of unity along the main diagonal that represent perfect correlation of each tract with itself. There are $p*(p-1)/2=66$ unique nontrivial elements in each matrix, which correspond to the symmetric pairwise correlations of the DTI parameter in each of the 12 tracts with the 11 other tracts.

To determine if there are statistically significant correlations of FA, MD, AD, and RD between white matter tracts, the 4 correlation matrices were tested for equivalence to the identity matrix and for equal correlations using the following two procedures from Rencher (2002). Consider the correlation matrix of a $p \times n$ data matrix, with n random samples from a p-dimensional normal distribution. The first null hypothesis is that the correlation matrix is the identity matrix, i.e., H_0: $\Sigma = \begin{bmatrix} 1 & 0 & \dots & 0 \\ 0 & 1 & \dots & 0 \\ & \dots & & \\ 0 & \dots & 0 & 1 \end{bmatrix}$. The test statistic is a modified likelihood ratio, $u_I = \upsilon[\ln|\Sigma_0| - \ln|S| + tr(S\Sigma_0^{-1}) - p]$, where $\upsilon = n-1$ is the degrees of freedom of the test, $\Sigma_0 = I$ is the hypothesized correlation matrix, S is the calculated sample correlation matrix, and $tr(\cdot)$ is the trace of a matrix. If H_0 is true, u is approximately distributed as $\chi^2\left[\frac{1}{2}p(p+1)\right]$, therefore, we reject the hypothesis if u_I is greater than $\chi^2\left[\alpha, \frac{1}{2}p(p+1)\right]$. We use a significance level of $\alpha=0.0125$, which represents a Bonferroni correction for four comparisons from the typical significance threshold of $\alpha=0.05$.

The second null hypothesis is that the correlation matrix has homogeneous structure, i.e., H_0: $\Sigma = \begin{bmatrix} 1 & \rho & \dots & \rho \\ \rho & 1 & \dots & \rho \\ & \dots & & \\ \rho & \dots & \rho & 1 \end{bmatrix}$, where $\rho>0$ is the common correlation coefficient among all variables. The test statistic is a likelihood ratio, $u_H = \frac{|S|}{(s^2)^p(1-r)^{p-1}[1+(p-1)r]}$ where S is the calculated sample correlation matrix, $s^2=1$ is the variance of each variable due to variance normalization, and $r = \frac{1}{p(p-1)}\sum_{j \neq k} s_{jk}$ is the estimated common correlation coefficient ρ. If H_0 is true, a modified test statistic $u'_H = -\left[\upsilon - \frac{p(p+1)^2(2p-3)}{6(p-1)(p^2+p-4)}\right]\ln u_H$ is approximately distributed according to $\chi^2\left[\frac{1}{2}p(p+1)-2\right]$, similarly, we reject the hypothesis if u'_H is greater than $\chi^2\left[\alpha, \frac{1}{2}p(p+1)-2\right]$ with $\alpha=0.0125$, which represents a Bonferroni correction for four comparisons from the typical significance threshold of $\alpha=0.05$.

Finally, after establishing that the pairwise inter-tract correlations are significantly different from zero and also significantly different from each other, hierarchical clustering methods were used to characterize the patterns of inter-tract correlation in each matrix. The quantity $1-\rho$, where ρ is the Spearman's rank correlation coefficient, was used as the measure of distance or "dissimilarity" between white matter tracts for the purpose of clustering. Hierarchical clustering employed the hclust function in R version 2.9.2 (http://sekhon.berkeley.edu/stats/html/hclust.html). This function proceeds by iterative agglomeration of the white matter tracts into successively larger groups based on the distance measure. The results are viewed as a dendrogram, which illustrates the fusions made at each successive stage of agglomeration. Average distance linkage was employed as the method of agglomeration. Average distance linkage defines the distance between groups as the average of distances between all pairs of objects, where each pair is made up of one object from each group. To characterize the uncertainty of the linkages in these dendrograms of correlational distances, a multiscale bootstrap was applied to the clustering with 100,000 repetitions of the analysis, using the pvclust function in R (Suzuki and Shimodaira, 2006). The multiscale bootstrap yields an approximately unbiased p-value for each linkage in hierarchical clustering (Shimodaira 2002; Shimodaira 2004), and its application to hierarchical clustering of correlational distances has been previously demonstrated (http://research.stowers-institute.org/efg/R/Visualization/cor-cluster/index.htm). This uncertainty is expressed as a percentage confidence level. For the purpose of this study, a 95% confidence level, corresponding to an approximately unbiased p-value of 0.05, was chosen as the threshold for statistical significance for the grouping of tracts. At 100,000 bootstrap repetitions, the standard error for estimation of the percentage confidence level for each cluster was less than 0.05%. For clusters with confidence levels greater than 90%, this standard error was less than 0.002%.

Results

Structural MR images of all subjects were interpreted by a board-certified neuroradiologist as being free of any morphological abnormalities of the brain. DTI tractography was successfully performed for all 12 white matter pathways in all 44 subjects, with the exception of

Table 1
Mean and standard deviation of tract-based DTI parameters. Mean diffusivity (MD), axial diffusivity (AD), and radial diffusivity (RD) are in units of 10^{-3} mm^2/s. Fractional anisotropy (FA) is dimensionless.

	FA	MD	AD	RD
CB left	0.565 ± 0.028	0.773 ± 0.028	1.334 ± 0.057	0.493 ± 0.030
CB right	0.522 ± 0.028	0.771 ± 0.028	1.268 ± 0.053	0.522 ± 0.029
AF left	0.517 ± 0.023	0.747 ± 0.028	1.211 ± 0.049	0.515 ± 0.030
AF right	0.490 ± 0.030	0.764 ± 0.028	1.211 ± 0.049	0.541 ± 0.033
IFO left	0.549 ± 0.026	0.797 ± 0.022	1.354 ± 0.036	0.519 ± 0.029
IFO right	0.534 ± 0.024	0.805 ± 0.023	1.347 ± 0.037	0.535 ± 0.027
ILF left	0.510 ± 0.028	0.811 ± 0.029	1.321 ± 0.044	0.556 ± 0.033
ILF right	0.497 ± 0.026	0.825 ± 0.031	1.325 ± 0.043	0.575 ± 0.033
UF left	0.489 ± 0.022	0.795 ± 0.026	1.269 ± 0.040	0.558 ± 0.026
UF right	0.470 ± 0.024	0.815 ± 0.026	1.276 ± 0.042	0.584 ± 0.026
CST left	0.587 ± 0.023	0.752 ± 0.019	1.328 ± 0.041	0.464 ± 0.023
CST right	0.575 ± 0.021	0.768 ± 0.019	1.340 ± 0.041	0.482 ± 0.020

the right arcuate fasciculus in four subjects. The means and standard deviations for the FA, MD, AD, and RD values for each tract are provided in Table 1. Left hemispheric tracts tended to have greater FA than their right hemispheric counterparts; this asymmetry was most pronounced for the dorsal cingulate bundle, as has been previously reported (Gong et al., 2005; Wakana et al., 2007). The generally lower RD values in the left-sided tracts also reflect their higher FA compared to the right cerebral hemisphere.

Spatial overlap between tracts in the same hemisphere was computed as the percentage of shared voxels, as specified in the Materials and methods. The only significant overlaps were found between the IFO and the ILF and between the IFO and the UF. The mean percent shared voxels between left IFO and left ILF was 10.7% ± 3.3% and that between left IFO and left UF was 11.0% ± 3.7%. The mean percent shared voxels between right IFO and right ILF was 11.4% ± 3.7% and that between right IFO and right UF was 7.3% ± 3.1%. Negligible degrees of overlap were seen between the AF and the ILF and between the ILF and the UF in each hemisphere, with 1% or fewer shared voxels.

Matrices for the Spearman's rank correlation coefficient ρ for each of the four DTI parameters are given in Tables 2–5, with the trivial values of unity along the main diagonal excluded. All of the computed correlation values were positive; there were no inverse correlations between white matter tracts for any of the DTI parameters. Each of the four correlation matrices was evaluated for equivalence to the identity matrix using the test statistic u_I, as detailed in the Materials and methods. The null hypothesis was rejected for all four matrices. The four subjects for whom the right arcuate fasciculus could not be tracked were excluded from this particular analysis since the test statistic u_I cannot be used with missing values. This is valid because, if a subset of a matrix differs from identity, then the entire matrix also differs from identity. The value of u_I for the FA correlation matrix was 310.6, corresponding to $p<0.0001$ for rejecting the null hypothesis. The value of u_I for the MD correlation matrix was 431.4, corresponding to $p<0.0001$. The value of u_I for the AD correlation matrix was 285.5, corresponding to $p<0.0001$. The value of u_I for the RD correlation matrix was 365.6, corresponding to $p<0.0001$. Hence, it is concluded that statistically significant correlations between tracts exist for all four DTI parameters.

Each of the four correlation matrices was evaluated for homogenous structure, implying equal correlations throughout the off-diagonal elements in the correlation matrix, using the test statistic u_H as detailed in the Materials and methods. The null hypothesis was rejected for all four matrices. The four subjects for whom the right arcuate fasciculus could not be tracked were excluded from this particular analysis since the test statistic u_H cannot be used with missing values. This is valid because, if a subset of a matrix deviates from homogenous structure, then the entire matrix also deviates from homogenous structure. The value of u_H for the FA correlation matrix was 141.6, corresponding to $p<0.0001$ for rejecting the null hypothesis. The value of u_H for the MD correlation matrix was 121.9, corresponding to $p<0.001$. The value of u_H for the AD correlation matrix was 109.5, corresponding to $p<0.01$. The value of u_H for the RD correlation matrix was 127.5, corresponding to $p<0.001$. Hence, it is concluded that there are statistically significant variations in inter-tract correlations for all four DTI parameters. Based on the test statistic u_H, FA was the DTI parameter with the greatest variation in inter-tract correlations and AD was the DTI parameter with the least variation. The range of inter-tract FA correlations was also the greatest among the four DTI parameters, with the lowest value of $\rho=0.15$ found between the right UF and the right CST and the highest value of $\rho=0.88$ observed between the left and right IFO.

After establishing that microstructural correlations between white matter tracts exist and have a statistically significant variation, specific patterns of inter-tract relationships were sought in the correlation matrices. For all of the correlation analyses described below, missing data points from the four subjects in whom the right AF could not be tracked were excluded on a case-wise basis, i.e. correlations between the right AF and other tracts were limited to those 40 subjects in which the right AF was tracked, but the full 44 subjects were still used to perform correlations between tracts other than the right AF. We begin with the FA correlation matrix because FA is widely accepted as the most sensitive measure of white matter microstructural integrity among the four DTI parameters examined herein. Unsurprisingly, homologous pathways of the left and right cerebral hemispheres had high correlation coefficients for FA; however, there was a wide disparity in the strengths of coupling (Fig. 2). The strongest correlation among homologous tracts was found between FA of the left and right IFO ($\rho=0.88$), whereas the weakest correlation was between the left and right AF ($\rho=0.50$). The relationship between FA of left and right CB was also relatively weak ($\rho=0.57$), with an intermediate correlation coefficient found between left and right CST($\rho=0.62$), and relatively stronger associations between left and right UF ($\rho=0.70$) and left and right ILF ($\rho=0.73$). As expected, FA correlation coefficients between non-homologous tracts were

Table 2
Matrix of Spearman's ρ-values for correlation of FA between white matter tracts.

	CB left	CB right	AF left	AF right	IFO left	IFO right	ILF left	ILF right	UF left	UF right	CST left
CB right	0.57										
AF left	0.53	0.41									
AF right	0.35	0.34	0.50								
IFO left	0.49	0.52	0.60	0.42							
IFO right	0.46	0.41	0.60	0.44	0.88						
ILF left	0.36	0.40	0.63	0.38	0.75	0.73					
ILF right	0.48	0.33	0.58	0.53	0.56	0.60	0.73				
UF left	0.44	0.47	0.57	0.47	0.70	0.64	0.57	0.44			
UF right	0.51	0.52	0.48	0.32	0.70	0.71	0.50	0.55	0.70		
CST left	0.19	0.18	0.25	0.19	0.25	0.18	0.26	0.16	0.27	0.16	
CST right	0.19	0.17	0.34	0.27	0.25	0.19	0.22	0.35	0.21	0.15	0.62

Table 3
Matrix of Spearman's ρ-values for correlation of MD between white matter tracts.

	CB left	CB right	AF left	AF right	IFO left	IFO right	ILF left	ILF right	UF left	UF right	CST left
CB right	0.53										
AF left	0.51	0.50									
AF right	0.30	0.40	0.64								
IFO left	0.43	0.46	0.72	0.57							
IFO right	0.19	0.29	0.46	0.44	0.68						
ILF left	0.45	0.40	0.78	0.46	0.74	0.53					
ILF right	0.25	0.37	0.58	0.63	0.60	0.68	0.63				
UF left	0.40	0.30	0.62	0.47	0.50	0.25	0.55	0.44			
UF right	0.15	0.40	0.39	0.38	0.36	0.46	0.48	0.61	0.61		
CST left	0.57	0.48	0.74	0.47	0.53	0.36	0.64	0.42	0.45	0.34	
CST right	0.49	0.46	0.75	0.53	0.66	0.55	0.66	0.58	0.39	0.41	0.78

generally lower than that between homologous tracts. Nevertheless, some of these non-homologous FA correlation coefficients exceeded those of the more weakly linked homologous tracts (Table 2, Fig. 2). There were five pairwise FA correlation coefficients between non-homologous pathways that were greater than or equal to 0.7: left ILF–left IFO ($\rho = 0.75$); left ILF–right IFO ($\rho = 0.73$); left UF–left IFO ($\rho = 0.70$); right UF–left IFO ($\rho = 0.70$); and right UF–right IFO ($\rho = 0.71$). The weakest FA correlation coefficients were almost uniformly found between the CST on either side and the five pairs of association fiber pathways (Table 2, Fig. 2). All values of ρ between CST and association tracts were less than 0.3 except for right CST–right ILF ($\rho = 0.35$) and right CST–left AF ($\rho = 0.34$). In contradistinction, all values of ρ among the association pathways were greater than 0.3. Similar to the findings in the FA correlation matrix, it can also be ascertained from the other three correlation matrices that homologous tracts had generally greater degrees of correlation than non-homologous tracts; however, for each DTI parameter, there were specific examples of non-homologous axonal pathways that were more strongly correlated than many, or even all, of the homologous ones.

To more systematically investigate the specific patterns of co-variation among white matter tracts, agglomerative hierarchical clustering using average distance linkage was applied to each of the four correlation matrices. The degree of uncertainty for each of the linkages was calculated from multiscale bootstrapping, with statistical significance at a 95% confidence level threshold which is equivalent to $\alpha = 0.05$. The resulting dendrogram for FA (Fig. 3) shows that there are three statistically significant clusters at a confidence level of 95% or greater. Since FA in the left and right IFO had the strongest correlation of any two tracts ($\rho = 0.88$), they represent the first linkage in the hierarchical clustering, with a statistical significance level approaching 100%. The left and right CST also represented a significant cluster at a virtually 100% confidence level. Furthermore, the ten association tracts formed a statistically significant grouping distinct from the bilateral CST at a 99% confidence level. Hence, the paired corticospinal tracts represent an outgroup that was found to be the most dissimilar of the twelve white matter pathways based on the FA correlation matrix. This partition between the association and projection tracts resulted naturally from the large FA correlational distances between the bilateral CST and the other ten axonal pathways. Of the ten association tracts, the cingulum bundles were the most distant outgroup; this pair of limbic association tracts clustered separately from the eight neocortical association pathways at an 85% confidence level. Homologous tracts of the left and right cerebral hemispheres had shorter FA correlational distances than those between most non-homologous tracts, with certain exceptions such as for the left ILF, which was more closely related to the left IFO and the right IFO than to the right ILF with at least a 91% confidence level.

The dendrogram of MD correlational distances (Fig. 4) showed some similarities to the FA dendrogram, but also many important differences. Again, homologous tracts tended to form pairs, with the bilateral CST forming a statistically significant cluster at a 97% confidence level. However, the other two significant clusters were of mostly non-homologous tracts, specifically the left IFO with the left AF and the left ILF, as well as the bilateral CST with the aforementioned three pathways. The bilateral CB constituted the most distant outgroup by MD correlational distances, with the bilateral UF as the second most distant outgroup. The bilateral IFO, which was so tightly coupled by FA values, showed a relatively large MD correlational distance.

The dendrogram of AD correlational distances (Fig. 5) did not have any statistically significant clusters at the 95% confidence level, likely due to a more homogenous correlation matrix structure than for FA or MD, as also reflected by the u_{H} test statistic results reported above. The configuration of the AD dendrogram resembled that of the MD dendrogram more than the FA dendrogram, with the bilateral CB and the bilateral UF comprising the first and second most distant outgroups, respectively. The RD dendrogram (Fig. 6) also did not show any significant clusters; however, the bilateral CST approached significance as a cluster at the 94% confidence level and the ten association tracts also formed a nearly significant cluster at the 94%

Table 4
Matrix of Spearman's ρ-values for correlation of AD between white matter tracts.

	CB left	CB right	AF left	AF right	IFO left	IFO right	ILF left	ILF right	UF left	UF right	CST left
CB right	0.58										
AF left	0.33	0.43									
AF right	0.24	0.24	0.66								
IFO left	0.38	0.38	0.74	0.51							
IFO right	0.23	0.27	0.48	0.37	0.65						
ILF left	0.34	0.24	0.63	0.49	0.48	0.33					
ILF right	0.25	0.31	0.41	0.62	0.46	0.49	0.53				
UF left	0.23	0.29	0.57	0.49	0.71	0.43	0.38	0.39			
UF right	0.32	0.55	0.34	0.44	0.56	0.41	0.25	0.40	0.73		
CST left	0.04	0.02	0.55	0.45	0.30	0.29	0.46	0.34	0.35	0.08	
CST right	0.18	0.28	0.62	0.60	0.40	0.31	0.60	0.38	0.37	0.31	0.69

Table 5
Matrix of Spearman's ρ-values for correlation of RD between white matter tracts.

	CB left	CB right	AF left	AF right	IFO left	IFO right	ILF left	ILF right	UF left	UF right	CST left
CB right	0.58										
AF left	0.57	0.56									
AF right	0.44	0.55	0.57								
IFO left	0.48	0.72	0.63	0.65							
IFO right	0.42	0.58	0.50	0.60	0.81						
ILF left	0.44	0.71	0.76	0.59	0.77	0.73					
ILF right	0.41	0.46	0.62	0.65	0.59	0.66	0.69				
UF left	0.60	0.58	0.66	0.49	0.62	0.53	0.66	0.52			
UF right	0.43	0.47	0.42	0.38	0.52	0.64	0.57	0.66	0.59		
CST left	0.49	0.45	0.49	0.26	0.44	0.27	0.36	0.22	0.48	0.28	
CST right	0.33	0.37	0.47	0.42	0.45	0.31	0.32	0.47	0.36	0.25	0.62

confidence level. This partitioning of the projection tracts from the association tracts in the RD dendrogram was similar to the FA dendrogram. Another point of correspondence between the FA and RD dendrograms was that the left and right IFO were linked by the first edge since they had the shortest correlational distance among all tracts for both of these DTI parameters.

Discussion

Specific patterns of microstructural correlation in the human brain

In this initial survey of microstructural correlations among white matter tracts of the human brain, we have established that there are statistically significant inter-tract correlations across normal adults in tract-based measures of FA, MD, AD, and RD. Furthermore, there are statistically significant differences in the strength of these pairwise correlations, meaning that DTI parameters in some pairs of tracts are more tightly correlated than in others. Finally, we used hierarchical clustering of correlational distances to form a dendrogram of microstructural relationships among the examined axonal pathways for each DTI parameter, with multiscale bootstrapping of the results to estimate the uncertainty in the linkages of the dendrogram. This is a data-driven analysis method that, combined with the nonparametric Spearman's rank correlation coefficient as the distance measure, makes minimal assumptions about the underlying diffusion tensor imaging measurements.

These dendrograms showed that many, but not all, of the strongest correlations were between homologous tracts in the left and right hemispheres. Furthermore, even among homologous pairs of tracts, there were wide variations in the degree of coupling. The left and right

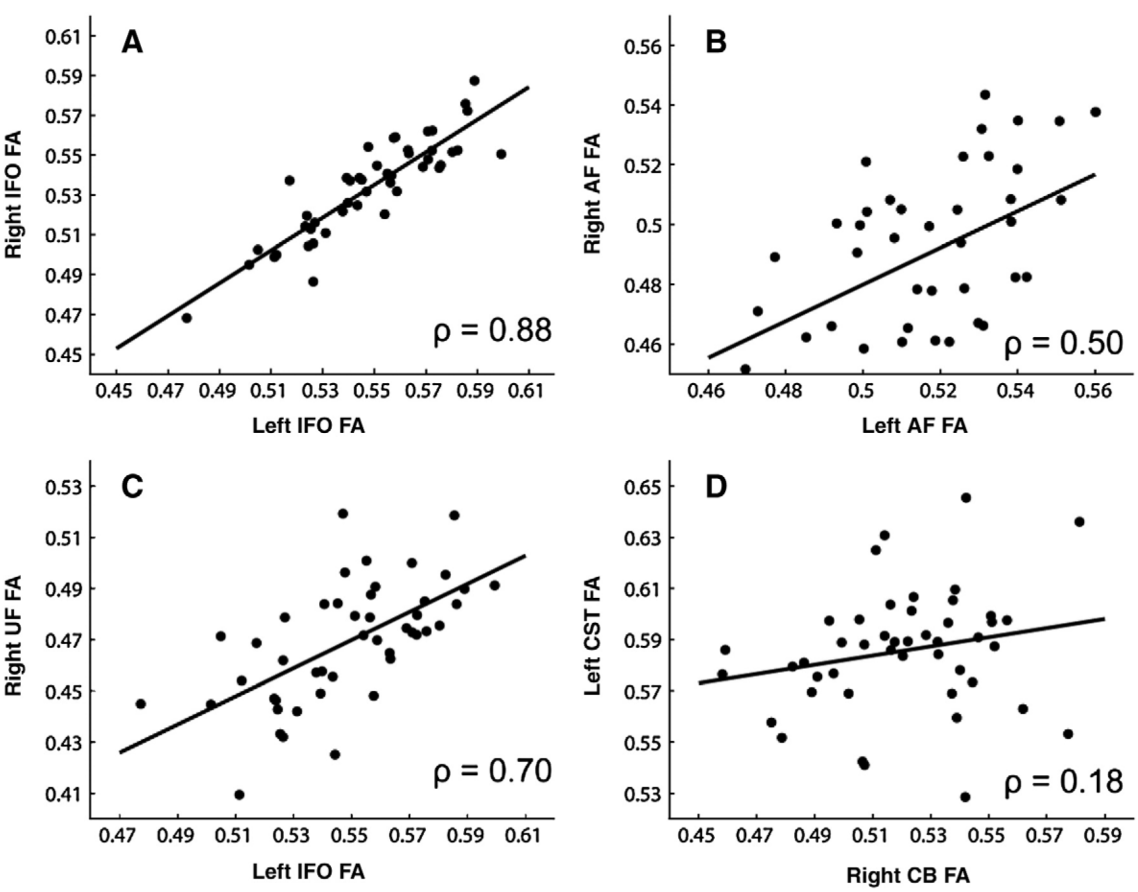

Fig. 2. Scatterplots of FA values show wide variation of inter-tract correlations between homologous pairs (A, B) and non-homologous pairs (C, D), as measured by the Spearman rank correlation coefficient ρ. The left and right IFO (A) are the most strongly correlated tracts among the 12 tracts studied. However, the FA correlation between the right UF and left IFO (C) exceeds that between a homologous pair, the left and right AF (B). The correlation between a projection tract, the left CST, and an association tract such as the right CB, is very weak (D).

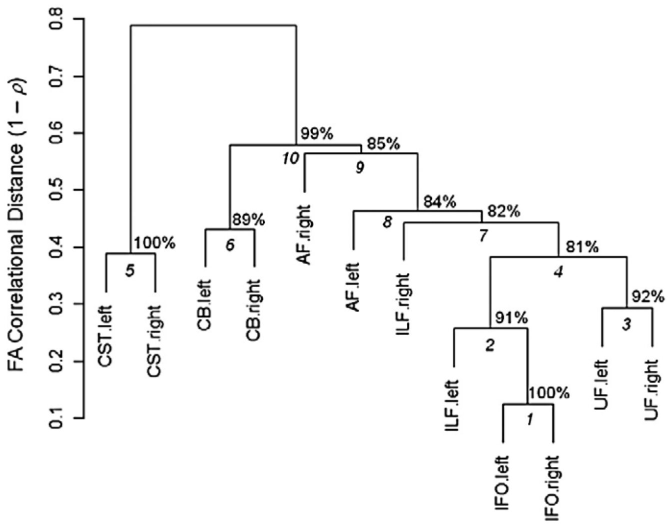

Fig. 3. Hierarchical clustering of FA correlational distances displayed as a dendrogram. The distance measure is $1-\rho$, where ρ is the Spearman rank correlation coefficient. The statistical confidence level of each linkage in the dendrogram is given as a percentage above the edge representing the linkage. For example, there is a 92% confidence level that the left and right UF form a cluster. The edge number, reflecting the order in which the linkages were formed during agglomeration of the groups, is given in italics below each edge. For example, the left and right IFO were the first tracts to be linked into a cluster by the hierarchical clustering algorithm.

inferior fronto-occipital fasciculi in particular were the most tightly correlated pair of tracts in terms of their FA ($\rho=0.88$) and RD ($\rho=0.81$). The weakest FA correlations between homologous tracts were found between the left and right arcuate fasciculi ($\rho=0.50$), with the right AF forming an outgroup compared to the other seven neocortical association pathways. This might reflect the well-known structural and functional hemispheric asymmetry of the AF, with the left AF showing larger size and greater FA values in most individuals (Powell et al., 2006; Catani et al., 2007; Rodrigo et al., 2007; Wakana et al., 2007), the latter also demonstrated in Table 1. Evidence that this macrostructural and microstructural asymmetry in the AF is related to left hemispheric language specialization is provided by a study showing that greater leftward FA lateralization correlated with stronger left-sided dominance for language activation on fMRI (Powell et al., 2006). Interestingly, the IFO is thought to be a phylogenetically novel tract in humans which is not found in non-human primates,

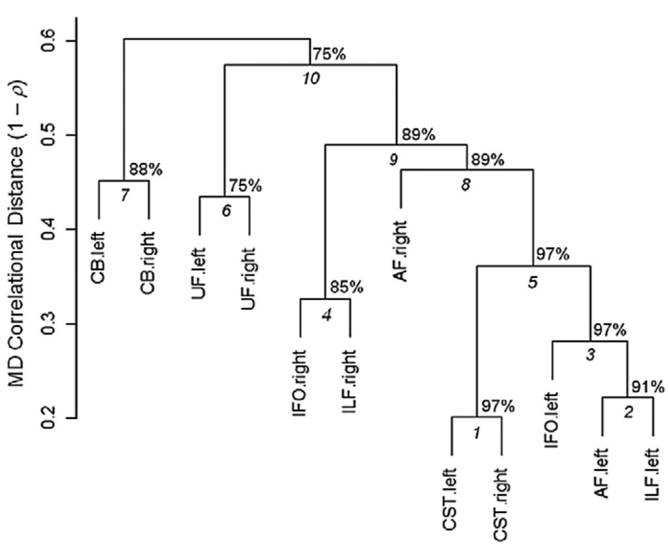

Fig. 4. Hierarchical clustering of MD correlational distances displayed as a dendrogram. All conventions are as in Fig. 3.

whereas the AF may have derived from the further elaboration and left lateralization of a perisylvian white matter network present in apes (Catani, 2006; Catani, 2007). It is known that the right AF causes greater difficulties for DTI tractography than is encountered with the left AF, often resulting in the asymmetrically small size of the computed right AF fiber tracks (Wakana et al., 2007). It is not clear the extent to which the smaller size of the right AF fiber tracks has its basis in underlying gross anatomic and microstructural differences with the left AF. The right AF may not be found at all by DTI tractography in some healthy adults (Catani et al., 2007). In our cohort, the right AF was not trackable in four subjects; these missing data points were excluded from the correlation analyses. Additionally, the CB showed relatively weak inter-hemispheric correlation for FA ($\rho=0.57$), which may also reflect the known functional and microstructural hemispheric asymmetry between these tracts as reflected in the higher average FA for the left CB than the right CB (Gong et al., 2005; Wakana et al., 2007).

Another major finding of our study was the strong degree of microstructural correlation between specific non-homologous white matter pathways. Indeed, some of these heterologous associations were stronger than those between most homologous pairs of tracts. In the dendrograms, these heterologous relationships are reflected as shorter correlational distances between non-homologous tracts than between some homologous pairs. For FA values, particularly strong non-homologous correlations were found between IFO, ILF, and UF both within and across hemispheres. These findings that correlations of DTI parameters between certain pairs of homologous tracts are weaker than those between specific non-homologous tracts call into question the increasingly common practice in the DTI literature of using the contralateral tract as a control for the ipsilateral homologous tract in clinical studies where the pathology is presumed to be unilateral, for example in traumatic brain injury (Mayer et al., 2010). Even besides the known hemispheric asymmetry of the mean FA values of tracts such as the AF and the CB (Gong et al., 2005; Wakana et al., 2007), the relatively weak inter-hemispheric microstructural correlations of these pathways means that there is no reason to expect that the contralateral tract would be particularly representative of the premorbid status of the tract ipsilateral to the pathology.

The pairwise correlations of FA values showed that the eight neocortical association pathways (four pairs: AF, IFO, ILF, and UF) formed a separate cluster from the two limbic association pathways (left and right CB). Also, the only non-association tracts (the left and right CST) constituted the most distant outgroup of the FA dendrogram. Hence, the correlational patterns of FA appear to reflect known phylogenetic and functional differences between white matter pathways. The partition between the two projection tracts and the ten association tracts was statistically significant at a 99% confidence level. The separation between the limbic and the neocortical association tracts reached trend-level significance at an 85% confidence level.

Among the four DTI parameters, FA showed the greatest variation in the strength of these pairwise correlations between white matter pathways. Also, the FA correlational matrix appeared to reflect known functional similarities and differences between tracts better than the other three DTI metrics. With a larger sample size, it seems likely that many of the linkages in the FA dendrogram that did not reach the 95% confidence level with the current cohort of 44 subjects would then become significant. FA has become the consensus measure of white matter microstructural “integrity” throughout the DTI literature due to its sensitivity to changes of maturation, senescence, and diverse forms of brain pathology in humans and in experimental animal models. However, even other DTI parameters that are thought to be less sensitive to white matter microstructural integrity than FA, such as the mean diffusivity, did show variations in inter-tract correlations that were manifested as statistically significant clusters in the dendrogram analysis. Importantly, there were differences between the

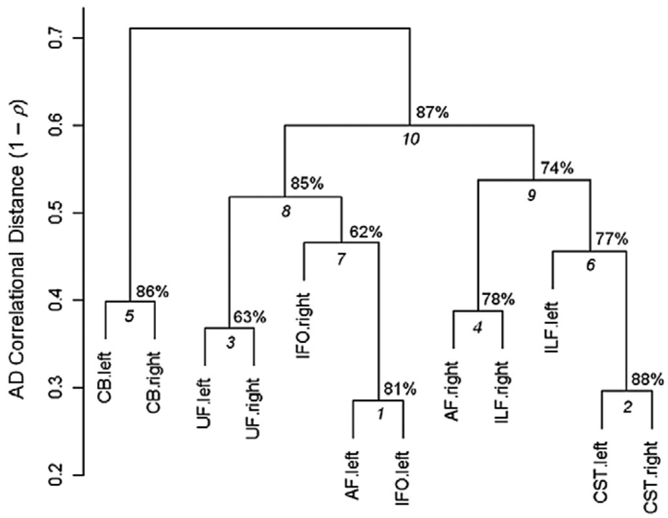

Fig. 5. Hierarchical clustering of AD correlational distances displayed as a dendrogram. All conventions are as in Fig. 3.

statistically significant groupings of tracts found with FA and with MD, suggesting that each metric may emphasize at least partially distinct microstructural properties of white matter pathways. Of course, the four DTI parameters that were examined herein do not provide completely independent information. In fact, the AD and RD are completely determined by the values of MD and FA, and vice versa (Hasan and Narayana, 2006). Therefore, it is anticipated that the AD and RD correlational structures share information with those of FA and MD. Diffusion anisotropy in large white matter tracts is reflected by the much lower values of the minor eigenvalues than the major eigenvalue. This prolate shape of the diffusion tensor emerges during human brain maturation from decreases in the two minor eigenvalues, i.e. the radial diffusivity, with relatively little change in the major eigenvalue, i.e. the axial diffusivity (Mukherjee et al., 2002). Conversely, dysmyelination has been shown in animal models to reduce anisotropy by preferentially increasing the radial diffusivity of white matter but not altering the axial diffusivity (Song et al., 2002). Hence, it might be expected that the RD dendrogram would more closely resemble FA than would the AD dendrogram. The relative lack of inter-tract correlational structure for AD suggests that it does not

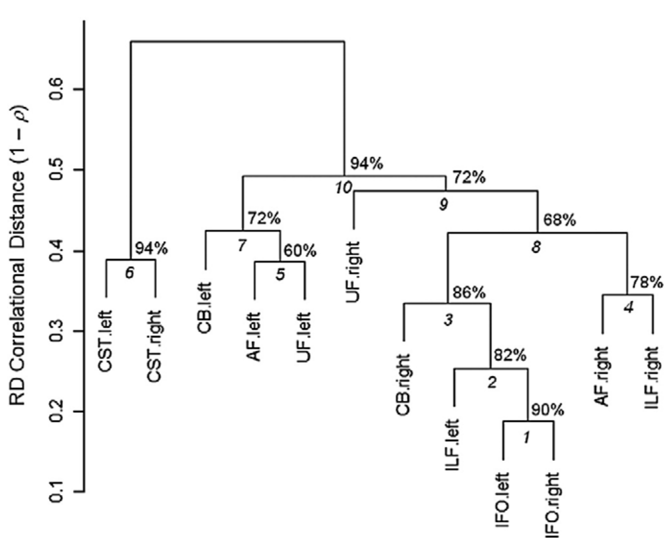

Fig. 6. Hierarchical clustering of RD correlational distances displayed as a dendrogram. All conventions are as in Fig. 3.

convey as much interesting white matter microstructural information as does FA or RD.

Possible substrates for white matter microstructural correlations

Clustering methods have previously been used in DTI studies for purposes such as the automatic segmentation of white matter tracts (Jonasson et al., 2005; O'Donnell et al., 2006; Awate et al., 2007; Hasan et al., 2007; Voineskos et al., 2009) and thalamic nuclei (Wiegell et al., 2003) as well as for unsupervised voxel-based tissue classification (Li et al., 2004; Wang and Vemuri, 2005; Freidlin et al., 2009). To our knowledge, this is the first investigation of correlations in white matter tract-based DTI parameters across individuals and the first to use these inter-tract correlations to determine whether there are specific microstructural relationships between fiber pathways. Hierarchical clustering analysis suggests that the strength of the observed correlations might reflect anatomic, phylogenetic, and/or functional similarities between tracts. This would explain why homologous tracts tended to cluster together, except in cases like the AF where known anatomic and functional hemispheric asymmetries exist. Phylogenetic and functional differences may also explain why neocortical and limbic association tracts group separately on the FA dendrogram, yet are more closely related to each other microstructurally than to a cortical–subcortical projection pathway such as the corticospinal tract.

The best current evidence is that the biophysical basis of white matter anisotropy is related to the effect of longitudinally oriented axonal membranes, the coherence of the parallel organization of axons within fibers, the packing density of the fibers, and their degree of myelination (Beaulieu, 2002). Presently, the question of which of these underlying biophysical substrates govern the microstructural relationships among different tracts remains unresolved and is worthy of further investigation in animal models. On the clinical side, there are many possible variables that might influence inter-tract correlations in the human brain. Demographic attributes such as age, gender, and intelligence quotient, among many other factors, may contribute to these microstructural relationships. These await future research on larger cohorts, in which such dependencies can be evaluated with adequate statistical power. Of these demographic variables, age is the one that has been best studied in the DTI literature (Pfefferbaum et al., 2000; Mukherjee et al., 2001; Salat et al., 2005; Snook et al., 2005; Hermoye et al., 2006). Based on what is known about the age dependence of the DTI parameters that we have investigated, it is unlikely to be the primary factor driving the correlations. Our sample consisted of adults from 20–50 years old, with a mean age of approximately 31 and a standard deviation of less than 8 years, so any effects of maturation or senescence would be minimized in the age range studied. Also, there is no known mechanism by which age or other demographic factors might produce the specific patterns of inter-tract correlations observed in this study.

Another potential cause of these microstructural correlations is spatial overlap in the course of the white matter tracts due to intravoxel partial volume averaging where two fiber pathways are in close proximity. The effects of partial volume averaging between tracts were minimized in this study by the relatively high spatial resolution of the DTI acquisition, with 1.8-mm voxels in all three dimensions, as well as the high angular resolution provided by 55 diffusion-weighted gradient directions, which serves to reduce error in the estimation of the principal diffusion tensor eigenvector at each voxel and enables more accurate fiber tracking (Jones 2004). Among the six pairs of tracts examined, regions of overlap were found between the IFO and the UF in the subinsular white matter (the external and extreme capsules), the temporal stem, and the inferior frontal lobe. An average of 7–11% of voxels were shared between the IFO and UF in each hemisphere. Spatial overlap between the IFO and ILF along the posterior aspect of their courses resulted in an average of 10–11% shared voxels in each hemisphere. While spatial overlap between these tracts may possibly contribute to the observed microstructural correlations, the low percentage of shared voxels and the high correlation coefficients show that it cannot be the decisive factor. Tables 2–5 show many instances of tracts correlating as well with non-homologous tracts of the contralateral hemisphere as with overlapping ipsilateral tracts. For example, the FA correlation between the left IFO and the left UF ($\rho = 0.70$), which have an average of 11% voxels in common, is identical to that between the left IFO and the right UF ($\rho = 0.70$), which have no shared voxels. Hence, if the high FA correlation between left IFO and left UF is explained only by spatial overlap, then the left and right UF would have to be perfectly correlated to account for the similarly high correlation between left IFO and right UF. Yet, the measured FA correlation between left and right UF is only at the same 0.70 level as that between left ILF and either UF.

It remains currently unresolved whether the microstructural correlations revealed herein are present from birth or whether they gradually develop during postnatal life. Studies of brain development in fetuses, newborns, infants, and children will hopefully elucidate the extent to which these findings are the result of genetic programming and how much may instead reflect usage-dependent neuroplasticity, perhaps even extending into adulthood and modulated over time by changes in cognition and other aspects of behavior. Under this hypothesis, long-term repetitive activation of brain networks subserving particular forms of cognition and behavior, or of the so-called resting state brain networks (Biswal et al., 1995; Greicius et al., 2003; Fox et al., 2005), may result in microstructural changes specific to the tracts interconnecting those networks. Variation in this network-based activity may drive inter-individual differences in tract-based DTI parameters that are correlated for pathways belonging to the same functional networks. This premise remains to be tested in studies of neuroplasticity that combine functional imaging with diffusion-based white matter microstructural analysis.

Future research directions

The study of microstructural correlations between white matter tracts might provide a new perspective with which to examine neurological and psychiatric diseases, including the effects of brain malformations, brain injury, and neurodegeneration. For example, in adults with agenesis of the corpus callosum, one might hypothesize that microstructural correlations between homologous tracts in the left and right cerebral hemispheres would be less than that in the normally formed brain due to the reduced inter-hemispheric functional connectivity that has been demonstrated in these acallosal subjects with both task activation and resting state fMRI (Quigley et al., 2003). In traumatic brain injury, reduced FA has been reported in numerous white matter pathways (Arfanakis et al., 2002; Kraus et al. 2007; Niogi et al. 2008a) and injury to specific tracts is associated with particular cognitive deficits (Niogi et al. 2008b). It would be interesting to ascertain whether traumatic axonal injury reduces the microstructural correlations seen in the uninjured brain, or whether networks of tracts correlated at the microstructural level might show synchronous post-traumatic degeneration. Similarly, recent work in neurodegenerative disorders using functional connectivity fMRI techniques has emphasized the importance of network-based neurodegeneration, with involvement of distinct cortical networks for each type of clinical disorder such as Alzheimer disease and frontotemporal dementia (Seeley et al. 2009). The examination of altered microstructural correlations in the affected white matter pathways could add a new dimension to the pathophysiological understanding of neurodegenerative diseases.

Knowledge of the underlying correlation structure of white matter microarchitecture should aid studies of the effect of white matter on cognition and behavior, as well as studies of genetic influences on white matter microstructure (Nierenberg et al., 2005; Persson et al., 2006; McIntosh et al., 2008; Winterer et al., 2008; Chiang et al., 2009). In particular, microstructural correlation matrices might be useful as prior information for Bayesian inferences in relating genes to white matter and in relating white matter to cognition and behavior. For these purposes, maps of white matter correlational structure at a finer spatial scale than that of whole tracts, such as at the voxel level, would be more powerful. However, voxel-level correlation matrices would have vastly greater dimensionality than those from tract-based measures, and would therefore require much larger datasets to provide statistically significant information. The recently developed tract-based morphometry approach (O'Donnell et al., 2009) might represent a more practical alternative, as it has already been used to reveal regions within the left and right CB that have statistically significant microstructural asymmetry between hemispheres. This methodology might be extended to explore more generally microstructural correlations at a spatial scale less than that of whole tracts. Of note, our study explored correlations using univariate scalar quantities derived from the diffusion tensor, such as FA and MD. More microstructural information might be obtained about human white matter architecture by employing a tensor-variate measure of distance instead (Pasternak et al., 2010). This is another promising avenue for further investigation.

Study limitations

This initial survey of the microstructural correlation patterns of the human brain was limited by modest sample size ($n = 44$). The number of subjects was sufficient to achieve the three primary objectives of this study: (1) to determine that there are statistically significant microstructural correlations among white matter tracts, (2) to establish that there are statistically significant variations in these microstructural correlations, and (3) to use these variations to preliminarily group the fiber tracts based on relatedness of microarchitecture. However, the number of white matter tracts that could be examined was constrained by the size of the cohort, since the number of pairwise comparisons increases quadratically with the number of pathways, rapidly leading to a loss of statistical power. Therefore, we chose to limit our evaluation to six pairs of white matter tracts which have diverse phylogenetic origins and functions, which can be compared across hemispheres, and for which reproducible quantitative fiber tracking protocols have been established (Wakana et al., 2007; Danielian et al., 2010). Although statistically significant groupings of the tracts could be ascertained from hierarchical clustering analysis of the FA and MD correlation matrices, those linkages with greater degrees of uncertainty in all four DTI correlational matrices must be regarded as provisional until confirmed by a larger-scale study. Furthermore, the statistical confidence levels of the four dendrograms were not corrected for multiple comparisons, one for each of the DTI parameters, in the absence of any known principled way to correct dendrograms for multiple comparisons across correlated variables such as FA, MD, AD, and RD. However, the central result that the two projection pathways cluster separately from the ten association pathways for FA has strong enough statistical confidence to survive even Bonferroni correction for the four comparisons. It is also important to note that the dendrogram structure for DTI parameters that are known to be highly correlated (e.g. FA and RD) are more similar than for DTI parameters that are less strongly associated (e.g. FA and MD). We believe that this correspondence represents further evidence for the accuracy of the clustering results.

This investigation was also limited by the rank-2 tensor model of diffusion, which has well-known shortcomings for tractography in regions of complex white matter architecture such as intravoxel crossing fibers (Frank, 2001; Tuch, 2004). For example, the laterally oriented motor fibers representing the face and arm are typically not trackable using DTI; hence, CST tractography is limited to the motor representation of the lower half of the body, located at the vertex of the primary motor cortex (Fig. 1F). Moreover, errors in fiber tracking due to intravoxel partial volume averaging of fiber populations with different orientations could potentially lead to sampling of non-equivalent portions of tracts across different subjects, which would be expected to artifactually reduce the measured microstructural correlations by introducing another source of variation. These problems could potentially be overcome by using fiber tracking based on newer mathematical models that do not assume Gaussian diffusion, such as *q*-ball imaging (Tuch, 2004; Hess et al., 2006; Barnett, 2009; Canales-Rodríguez et al., 2009), spherical deconvolution (Tournier et al., 2004), and the diffusion orientation transform (Ozarslan et al., 2006), to name a few. Extending the diffusion measurements to multiple *b*-values, including values well in excess of the 1000 s/mm^2 used in this study, would permit full or hybrid *q*-space analysis (Cohen and Assaf, 2002; Wedeen et al., 2005; Wu and Alexander, 2007) combined with biophysical modeling (Assaf and Basser, 2005; Assaf et al., 2008) that may yield more and better microstructural parameters for correlational analysis than could be obtained from DTI.

Conclusion

Taken together, these initial results from DTI correlation analysis provide evidence for our hypotheses that specific relationships exist in the microstructural organization of different white matter pathways beyond those of homologous pairs of tracts in the two cerebral hemispheres, and that these relationships may reflect phylogenetic and/or functional similarities between tracts. Further studies of inter-tract DTI correlations encompassing many more pathways in a larger cohort will likely provide a wealth of novel and interesting information about the architecture of human brain networks, especially in combination with functional connectivity data from fMRI (Biswal et al., 1995; Greicius et al., 2003; Fox et al., 2005) as well as macrostructural covariance data from structural MRI measures of regional cortical thickness (He et al., 2007). Greater knowledge of the microstructural relationships between white matter pathways might aid studies of the genetics and of the behavioral effects of white matter architecture, as well as provide a revealing new perspective with which to investigate neurologic disorders such as brain malformations, brain injury, and neurodegeneration.

Acknowledgments

This study was supported by grants from the James S. McDonnell Foundation, the Charles A. Dana Foundation, the American Society of Neuroradiology, the U.S. National Institutes of Health (R01 NS060776), and the Academic Senate of the University of California, San Francisco. The authors would like to thank Ryota Suzuki for helpful discussions on hierarchical data clustering and for providing R code modifications for the pvclust algorithm to enable the Spearman's rank correlation coefficient as a distance measure.

References

Arfanakis, K., Haughton, V.M., Carew, J.D., Rogers, B.P., Dempsey, R.J., Meyerand, M.E., 2002. Diffusion tensor MR imaging in diffuse axonal injury. AJNR Am. J. Neuroradiol. 23, 794–802.
Assaf, Y., Basser, P.J., 2005. Composite hindered and restricted model of diffusion (CHARMED) MR imaging of the human brain. Neuroimage 27, 48–58.
Assaf, Y., Blumenfeld-Katzir, T., Yovel, Y., Basser, P.J., 2008. AxCaliber: a method for measuring axon diameter distribution from diffusion MRI. Magn. Reson. Med. 59, 1347–1354.
Awate, S.P., Zhang, H., Gee, J.C., 2007. A fuzzy, nonparametric segmentation framework for DTI and MRI analysis: with applications to DTI-tract extraction. IEEE Trans. Med. Imaging 26, 1525–1536.
Barnett, A., 2009. Theory of Q-ball imaging redux: implications for fiber tracking. Magn. Reson. Med. 62, 910–923.
Basser, P.J., Pierpaoli, C., 1996. Microstructural and physiological features of tissues elucidated by quantitative diffusion tensor MRI. J. Magn. Reson. B 111, 209–219.
Basser, P.J., Pajevic, S., Pierpaoli, C., Duda, J., Aldroubi, A., 2000. In vivo fiber tractography using DT-MRI data. Magn. Reson. 44, 625–632.
Beaulieu, C., 2002. The basis of anisotropic water diffusion in the nervous system — a technical review. NMR Biomed. 15, 435–455.
Beaulieu, C., Pewes, C., Paulson, L.A., Roy, D., Snook, L., Concha, L., Phillips, L., 2005. Imaging brain connectivity in children with diverse reading ability. Neuroimage 25, 1266–1271.
Biswal, B., Yetkin, F.Z., Haughton, V.M., Hyde, J.S., 1995. Functional connectivity in the motor cortex of resting human brain using echo-planar MRI. Magn. Reson. Med. 34, 537–541.
Bonekamp, D., Nagae, L.M., Degaonkar, M., Matson, M., Abdalla, W.M., Barker, P.B., Mori, S., Horská, A., 2007. Diffusion tensor imaging in children and adolescents: reproducibility, hemispheric, and age-related differences. Neuroimage 34, 733–742.
Canales-Rodríguez, E.J., Melie-García, L., Iturria-Medina, Y., 2009. Mathematical description of q-space in spherical coordinates: exact q-ball imaging. Magn. Reson. Med. 61, 1350–1367.
Catani, M., 2006. Diffusion tensor magnetic resonance imaging tractography in cognitive disorders. Curr. Opin. Neurol. 19, 599–606.
Catani, M., 2007. From hodology to function. Brain 130, 602–605.
Catani, M., Allin, M.P., Husain, M., Pugliese, L., Mesulam, M.M., Murray, R.M., Jones, D.K., 2007. Symmetries in human brain language pathways correlate with verbal recall. Proc. Natl. Acad. Sci. U. S. A. 104, 17163–17168.
Chiang, M.C., Barysheva, M., Shattuck, D.W., Lee, A.D., Madsen, S.K., Avedissian, C., Klunder, A.D., Toga, A.W., McMahon, K.L., de Zubicaray, G.I., Wright, M.J., Srivastava, A., Balov, N., Thompson, P.M., 2009. Genetics of brain fiber architecture and intellectual performance. J. Neurosci. 29, 2212–2224.
Cohen, Y., Assaf, Y., 2002. High *b*-value *q*-space analyzed diffusion-weighted MRS and MRI in neuronal tissues — a technical review. NMR Biomed. 15, 516–542.
Conturo, T.E., Lori, N.F., Cull, T.S., Akbudak, E., Snyder, A.Z., Shimony, J.S., McKinstry, R.C., Burton, H., Raichle, M.E., 1999. Tracking neuronal fiber pathways in the living human brain. Proc. Natl. Acad. Sci. U. S. A. 96, 10422–10427.
Danielian, L.E., Iwata, N.K., Thomasson, D.M., Floeter, M.K., 2010. Reliability of fiber tracking measurements in diffusion tensor imaging for longitudinal study. Neuroimage. 49, 1572–1580.
Dietrich, O., Raya, J.G., Reeder, S.B., Reiser, M.F., Schoenberg, S.O., 2007. Measurement of signal-to-noise ratios in MR images: influence of multichannel coils, parallel imaging, and reconstruction filters. J. Magn. Reson. Imaging 26, 375–385.
Fox, M.D., Snyder, A.Z., Vincent, J.L., Corbetta, M., Van Essen, D.C., Raichle, M.E., 2005. The human brain is intrinsically organized into dynamic, anticorrelated functional networks. Proc. Natl. Acad. Sci. U. S. A. 102, 9673–9678.
Frank, L.R., 2001. Anisotropy in high angular resolution diffusion-weighted MRI. Magn. Reson. Med. 45, 935–939.
Freidlin, R.Z., Ozarslan, E., Assaf, Y., Komlosh, M.E., Basser, P.J., 2009. A multivariate hypothesis testing framework for tissue clustering and classification of DTI data. NMR Biomed. 22, 716–729.
Greicius, M.D., Krasnow, B., Reiss, A.L., Menon, V., 2003. Functional connectivity in the resting brain: a network analysis of the default mode hypothesis. Proc. Natl. Acad. Sci. U. S. A. 100, 253–258.
Gong, G., Jiang, T., Zhu, C., Zang, Y., He, Y., Xie, S., Xiao, J., 2005. Side and handedness effects on the cingulum from diffusion tensor imaging. Neuroreport 16, 1701–1705.
Hasan, K.M., Narayana, P.A., 2006. Retrospective measurement of the diffusion tensor eigenvalues from diffusion anisotropy and mean diffusivity in DTI. Magn. Reson. Med. 56, 130–137.
Hasan, K.M., Halphen, C., Sankar, A., Eluvathingal, T.J., Kramer, L., Stuebing, K.K., Ewing-Cobbs, L., Fletcher, J.M., 2007. Diffusion tensor imaging-based tissue segmentation: validation and application to the developing child and adolescent brain. Neuroimage 34, 1497–1505.
He, Y., Chen, Z.J., Evans, A.C., 2007. Small-world anatomical networks in the human brain revealed by cortical thickness from MRI. Cereb. Cortex 17, 2407–2419.
Hermoye, L., Saint-Martin, C., Cosnard, G., Lee, S.K., Kim, J., Nassogne, M.C., Menten, R., Clapuyt, P., Donohue, P.K., Hua, K., Wakana, S., Jiang, H., van Zijl, P.C., Mori, S., 2006. Pediatric diffusion tensor imaging: normal database and observation of the white matter maturation in early childhood. Neuroimage 29, 493–504.
Hess, C.P., Mukherjee, P., Han, E.T., Xu, D., Vigneron, D.B., 2006. Q-ball reconstruction of multimodal fiber orientations using the spherical harmonic basis. Magn. Reson. Med. 56, 104–117.
Jenkinson, M., Bannister, P., Brady, M., Smith, S., 2002. Improved optimization for the robust and accurate linear registration and motion correction of brain images. Neuroimage 17, 825–841.
Jiang, H., van Zijl, P.C., Kim, J., Pearlson, G.D., Mori, S., 2006. DtiStudio: resource program for diffusion tensor computation and fiber bundle tracking. Comput. Methods Programs Biomed. 81, 106–116.
Jonasson, L., Bresson, X., Hagmann, P., Cuisenaire, O., Meuli, R., Thiran, J.P., 2005. White matter fiber tract segmentation in DT-MRI using geometric flows. Med. Image Anal. 9, 223–236.
Jones, D.K., 2004. The effect of gradient sampling schemes on measures derived from diffusion tensor MRI: a Monte Carlo study. Magn. Reson. Med. 51, 807–815.
Klingberg, T., Hedehus, M., Temple, E., Salz, T., Gabrieli, J.D., Moseley, M.E., Poldrack, R.A., 2000. Microstructure of temporo-parietal white matter as a basis for reading ability: evidence from diffusion tensor magnetic resonance imaging. Neuron 25, 493–500.
Kraus, M.F., Susmaras, T., Caughlin, B.P., Walker, C.J., Sweeney, J.A., Little, D.M., 2007. White matter integrity and cognition in chronic traumatic brain injury: a diffusion tensor imaging study. Brain 130, 2508–2519.
Li, W., Tian, J., Li, E., Dai, J., 2004. Robust unsupervised segmentation of infarct lesion from diffusion tensor MR images using multiscale statistical classification and partial volume voxel reclassification. Neuroimage 23, 1507–1518.

Li, Z., Moore, A.B., Tyner, C., Hu, X., 2009. Asymmetric connectivity reduction and its relationship to “HAROLD” in aging brain. Brain Res. 1295, 149–158.

Mayer, A.R., Ling, J., Mannell, M.V., Gasparovic, C., Phillips, J.P., Doezema, D., Reichard, R., Yeo, R.A., 2010. A prospective diffusion tensor imaging study in mild traumatic brain injury. Neurology 74, 643–650.

McIntosh, A.M., Moorhead, T.W., Job, D., Lymer, G.K., Muñoz Maniega, S., McKirdy, J., Sussmann, J.E., Baig, B.J., Bastin, M.E., Porteous, D., Evans, K.L., Johnstone, E.C., Lawrie, S.M., Hall, J., 2008. The effects of a neuregulin 1 variant on white matter density and integrity. Mol. Psychiatry 13, 1054–1059.

Mori, S., Crain, B.J., Chacko, V.P., van Zijl, P.C.M., 1999. Three-dimensional tracking of axonal projections in the brain by magnetic resonance imaging. Ann. Neurol. 45, 265–269.

Mori, S., Wakana, S., van Zijl, P.C.M., 2005. MRI Atlas of Human White Matter. Elsevier.

Mukherjee, P., Miller, J.H., Shimony, J.S., Conturo, T.E., Lee, B.C., Almli, C.R., McKinstry, R.C., 2001. Normal brain maturation during childhood: developmental trends characterized with diffusion-tensor MR imaging. Radiology 221, 349–358.

Mukherjee, P., Miller, J.H., Shimony, J.S., Philip, J.V., Nehra, D., Snyder, A.Z., Conturo, T.E., Neil, J.J., McKinstry, R.C., 2002. Diffusion-tensor MR imaging of gray and white matter development during normal human brain maturation. AJNR Am. J. Neuroradiol. 23, 1445–1456.

Nierenberg, J., Pomara, N., Hoptman, M.J., Sidtis, J.J., Ardekani, B.A., Lim, K.O., 2005. Abnormal white matter integrity in healthy apolipoprotein E epsilon4 carriers. Neuroreport 16, 1369–1372.

Niogi, S.N., McCandliss, B.D., 2006. Left lateralized white matter microstructure accounts for individual differences in reading ability and disability. Neuropsychologia 44, 2178–2188.

Niogi, S.N., Mukherjee, P., Ghajar, J., Johnson, C.E., Kolster, R., Lee, H., Suh, M., Zimmerman, R.D., Manley, G.T., McCandliss, B.D., 2008a. Extent of microstructural white matter injury in postconcussive syndrome correlates with impaired cognitive reaction time: a 3 T diffusion tensor imaging study of mild traumatic brain injury. AJNR Am. J. Neuroradiol. 29, 967–973.

Niogi, S.N., Mukherjee, P., Ghajar, J., Johnson, C.E., Kolster, R., Lee, H., Suh, M., Zimmerman, R.D., Manley, G.T., McCandliss, B.D., 2008b. Structural dissociation of attentional control and memory in adults with and without mild traumatic brain injury. Brain 131, 3209–3221.

O'Donnell, L.J., Kubicki, M., Shenton, M.E., Dreusicke, M.H., Grimson, W.E., Westin, C.F., 2006. A method for clustering white matter fiber tracts. AJNR Am. J. Neuroradiol. 27, 1032–1036.

O'Donnell, L.J., Westin, C.F., Golby, A.J., 2009. Tract-based morphometry for white matter group analysis. Neuroimage 45, 832–844.

Ozarslan, E., Shepherd, T.M., Vemuri, B.C., Blackband, S.J., Mareci, T.H., 2006. Resolution of complex tissue microarchitecture using the diffusion orientation transform (DOT). Neuroimage 31, 1086–1103.

Pasternak, O., Sochen, N., Basser, P.J., 2010. The effect of metric selection on the analysis of diffusion tensor MRI data. Neuroimage 49, 2190–2204.

Persson, J., Lind, J., Larsson, A., Ingvar, M., Cruts, M., Van Broeckhoven, C., Adolfsson, R., Nilsson, L.G., Nyberg, L., 2006. Altered brain white matter integrity in healthy carriers of the APOE epsilon4 allele: a risk for AD? Neurology 66, 1029–1033.

Pfefferbaum, A., Sullivan, E.V., Hedehus, M., Lim, K.O., Adalsteinsson, E., Moseley, M., 2000. Age-related decline in brain white matter anisotropy measured with spatially corrected echo-planar diffusion tensor imaging. Magn. Reson. Med. 44, 259–268.

Pierpaoli, C., Jezzard, P., Basser, P.J., Barnett, A., Di Chiro, G., 1996. Diffusion tensor MR imaging of the human brain. Radiology 201, 637–648.

Powell, H.W., Parker, G.J., Alexander, D.C., Symms, M.R., Boulby, P.A., Wheeler-Kingshott, C.A., Barker, G.J., Noppeney, U., Koepp, M.J., Duncan, J.S., 2006. Hemispheric asymmetries in language-related pathways: a combined functional MRI and tractography study. Neuroimage 32, 388–399.

Quigley, M., Cordes, D., Turski, P., Moritz, C., Haughton, V., Seth, R., Meyerand, M.E., 2003. Role of the corpus callosum in functional connectivity. AJNR Am. J. Neuroradiol. 24, 208–212.

Reich, D.S., Smith, S.A., Jones, C.K., Zackowski, K.M., van Zijl, P.C., Calabresi, P.A., Mori, S., 2006. Quantitative characterization of the corticospinal tract at 3 T. AJNR Am. J. Neuroradiol. 27, 2168–2178.

Rencher, A.C., 2002. Methods of Multivariate Analysis, 2nd ed. Wiley Interscience, Hoboken, NJ.

Rodrigo, S., Naggara, O., Oppenheim, C., Golestani, N., Poupon, C., Cointepas, Y., Mangin, J.F., Le Bihan, D., Meder, J.F., 2007. Human subinsular asymmetry studied by diffusion tensor imaging and fiber tracking. AJNR Am. J. Neuroradiol. 28, 1526–1531.

Salat, D.H., Tuch, D.S., Greve, D.N., van der Kouwe, A.J., Hevelone, N.D., Zaleta, A.K., Rosen, B.R., Fischl, B., Corkin, S., Rosas, H.D., Dale, A.M., 2005. Age-related alterations in white matter microstructure measured by diffusion tensor imaging. Neurobiol. Aging 26, 1215–1227.

Seeley, W.W., Crawford, R.K., Zhou, J., Miller, B.L., Greicius, M.D., 2009. Neurodegenerative diseases target large-scale human brain networks. Neuron 62, 42–52.

Shimodaira, H., 2002. An approximately unbiased test of phylogenetic tree selection. Syst. Biol. 51, 492–508.

Shimodaira, H., 2004. Approximately unbiased tests of regions using multistep–multiscale bootstrap resampling. Ann. Stat. 32, 2616–2641.

Smith, S.M., 2002. Fast robust automated brain extraction. Human Brain Mapp. 17, 143–155.

Song, S.K., Sun, S.W., Ramsbottom, M.J., Chang, C., Russell, J., Cross, A.H., 2002. Dysmyelination revealed through MRI as increased radial (but unchanged axial) diffusion of water. Neuroimage 17, 1429–1436.

Snook, L., Paulson, L.A., Roy, D., Phillips, L., Beaulieu, C., 2005. Diffusion tensor imaging of neurodevelopment in children and young adults. Neuroimage 26, 1164–1173.

Suzuki, R., Shimodaira, H., 2006. Pvclust: an R package for assessing the uncertainty in hierarchical clustering. Bioinformatics 22, 1540–1542.

Tournier, J.D., Calamante, F., Gadian, D.G., Connelly, A., 2004. Direct estimation of the fiber orientation density function from diffusion-weighted MRI using spherical deconvolution. Neuroimage 23, 1176–1185.

Tuch, D.S., 2004. Q-ball imaging. Magn. Reson. Med. 52, 1358–1372.

Tuch, D.S., Salat, D.H., Wisco, J.J., Zaleta, A.K., Hevelone, N.D., Rosas, H.D., 2005. Choice reaction time performance correlates with diffusion anisotropy in white matter pathways supporting visuospatial attention. Proc. Natl. Acad. Sci. U. S. A. 102, 12212–12217.

Voineskos, A.N., O'Donnell, L.J., Lobaugh, N.J., Markant, D., Ameis, S.H., Niethammer, M., Mulsant, B.H., Pollock, B.G., Kennedy, J.L., Westin, C.F., Shenton, M.E., 2009. Quantitative examination of a novel clustering method using magnetic resonance diffusion tensor tractography. Neuroimage 45, 370–376.

Wakana, S., Caprihan, A., Panzenboeck, M.M., Fallon, J.H., Perry, M., Gollub, R.L., Hua, K., Zhang, J., Jiang, H., Dubey, P., Blitz, A., van Zijl, P., Mori, S., 2007. Reproducibility of quantitative tractography methods applied to cerebral white matter. Neuroimage 36, 630–644.

Wang, Z., Vemuri, B.C., 2005. DTI segmentation using an information theoretic tensor dissimilarity measure. IEEE Trans. Med. Imaging 24, 1267–1277.

Wedeen, V.J., Hagmann, P., Tseng, W.Y., Reese, T.G., Weisskoff, R.M., 2005. Mapping complex tissue architecture with diffusion spectrum magnetic resonance imaging. Magn. Reson. Med. 54, 1377–1386.

Wiegell, M.R., Tuch, D.S., Larsson, H.B., Wedeen, V.J., 2003. Automatic segmentation of thalamic nuclei from diffusion tensor magnetic resonance imaging. Neuroimage 19, 391–401.

Wilde, E.A., McCauley, S.R., Chu, Z., Hunter, J.V., Bigler, E.D., Yallampalli, R., Wang, Z.J., Hanten, G., Li, X., Ramos, M.A., Sabir, S.H., Vasquez, A.C., Menefee, D., Levin, H.S., 2009. Diffusion tensor imaging of hemispheric asymmetries in the developing brain. J. Clin. Exp. Neuropsychol. 31, 205–218.

Winterer, G., Konrad, A., Vucurevic, G., Musso, F., Stoeter, P., Dahmen, N., 2008. Association of 5′ end neuregulin-1 (NRG1) gene variation with subcortical medial frontal microstructure in humans. Neuroimage 40, 712–718.

Wu, Y.C., Alexander, A.L., 2007. Hybrid diffusion imaging. Neuroimage 36, 617–629.

Yasmin, H., Aoki, S., Abe, O., Nakata, Y., Hayashi, N., Masutani, Y., Goto, M., Ohtomo, K., 2009. Tract-specific analysis of white matter pathways in healthy subjects: a pilot study using diffusion tensor MRI. Neuroradiology 51, 831–840.

Zahr, N.M., Rohlfing, T., Pfefferbaum, A., Sullivan, E.V., 2009. Problem solving, working memory, and motor correlates of association and commissural fiber bundles in normal aging: a quantitative fiber tracking study. Neuroimage 44, 1050–1062.